Thrust Characterization of a Bioinspired Vortex Ring Thruster for Locomotion of Underwater Robots

Michael Krieg, *Student Member, IEEE*, and Kamran Mohseni, *Member, IEEE*

***Abstract*—A new type of thrusting technology, loosely inspired by the locomotion of cephalopods, offers promising low-speed maneuvering capabilities for a new generation of underwater vehicles and robots. The actuators consist of a small cavity with a moving wall on one side and an orifice on the other side. The net effect of periodic movement of the moving wall is the ingestion of low-momentum fluid inside the cavity and then the expulsion of the fluid as a pulsatile jet from the orifice, with no net mass flux. Continuous operation of the actuator results in a synthetic jet. The actuators provide a net positive momentum flux with zero net mass flux. They are compact with no extruding components to negatively impact the vehicle's drag at cruising speed. Parameters controlling the pulsatile jet and its thrust are identified. The thruster was empirically tested for a large range of frequencies and stroke ratios. The thrust characteristics of the device with respect to frequency was seen to converge to a single thrust coefficient. A model was developed to predict the thrust coefficient. The effect of the stroke ratios on the thrust coefficient is investigated. The model accurately predicts the observed thrust coefficient for stroke ratios up to five where the vortex ring pinchoff occurs. The accuracy of the model degrades for stroke ratios above the formation number where part of the expelled jet is pulled back into the cavity. Additionally, these devices have thrust tracking times faster than those reported for typical propellor-type thrusters, and deliver a fully quantized level of thrust.**

***Index Terms*—Autonomous underwater vehicle (AUV), propulsion, vortex ring.**

I. Introduction

THE overall design of underwater vehicles, like any engineering project, is principally defined by the intended use of the vehicle. Autonomous underwater vehicles (AUVs) serve a multitude of purposes including oceanographic observation, military surveillance, oil pipeline inspection, and search and rescue. The particular tasks that must be accomplished by these vehicles can vary quite drastically. Some studies, such as ocean floor mapping and remote sensing, require extremely accurate positioning and position sensing. This type of research is performed by vehicles like the Jason remotely operated vehicle (Jason ROV), which was developed by the Woods Hole Oceanographic Institution (Woods Hole, MA) for accurate ocean floor sensing and drilling. Other applications such as excavation of sunken wreckage require complete maneuvering capabilities in tight enclosed spaces. Since both testing environments are characterized by sporadic unpredictable currents, the vehicle's maneuvering systems must be capable of instantaneous uncoupled corrective propulsion [1]. To accomplish these capabilities, the traditional solution has been to create vehicles with multiple external thrusters at several locations around the vehicle. This solution has a limitation in that it gives the vehicle a very high drag profile and restricts overall velocity. Additionally, traditional propellor-type thrusters are very efficient when operating at nominal rotation rates. However, accurate positioning often requires short impulses, which correspond to propellor rotations in the order of single rotations, resulting in unpredictable control forces [2]. This coupled with the unpredictability of the environment causes traditional propellor-type thrusters to be nonideal for accurate maneuvering.

Other AUV applications involve oceanographic sensing on a much larger scale. These studies might focus on the trends in salinity, temperature, and velocity of ocean currents throughout the total ocean system, or they might involve monitoring biological and military activity throughout large regions. These applications require a network of autonomous vehicles with the capability to travel long distances in a very short period of time. Though the exact positioning of these vehicles is less important due to the resolution of global models, they do require a rapid travel time as well as long-range endurance so that the vehicles' characteristic survey time is below the cycling time associated with the study dynamics [3]. These vehicles are generally torpedo shaped and maneuver using control surfaces at very high velocities. Remote environmental measurement unit system (REMUS) is an excellent example of this type of vehicle. Control surfaces are effective at higher forward velocities. During the vehicle's launch or docking procedures, when the forward vehicle velocity drops, control surfaces will not be effective for maneuvering. Consequently, the current design of these vehicles appears to not be suitable for fully automated missions, such as inclusion in an automated ocean sampling network (AOSN) [4]–[6]. Vehicles have been designed utilizing tunnel thrusters, which run through the hull of the vehicle to give low-speed maneuvering capabilities to vehicles without compromising the forward drag profile. However, tunnel thrusters have been determined to be less effective when a cross flow is present; and they have been observed to continue producing a force even after being terminated [7].

There is an obvious contrast between the propulsive systems of typical naval vehicles (which are propellor dominated) and those developed through years of biological evolution. This dichotomy inspires the question as to whether a suitable compromise can be reached. Our group has developed a

Manuscript received September 21, 2007; accepted February 12, 2008. First published September 12, 2008; current version published October 31, 2008. This work was supported by the National Science Foundation.

Associate Editor: H. Maeda.

The authors are with the Aerospace Engineering Sciences, University of Colorado at Boulder, Boulder, CO 80309-429 USA (e-mail: mohseni@colorado.edu).

Color versions of one or more of the figures in this paper are available online at http://ieeexplore.ieee.org.

Digital Object Identifier 10.1109/JOE.2008.920171

vortex ring thruster (VRT) to mimic the propulsive technique of cephalopods and study the resulting thrust characteristics [8], [9]. Vortex rings are efficient at transporting momentum across long distances through the surrounding fluid medium, partially due to their inherent induction velocity. The large mass of the fluid jet itself results in a significant momentum transfer between the VRT and the encompassing fluid reservoir. VRT devices can be developed to have a positive momentum flux across their opening, with a null mass flux over an entire actuation cycle.

The recent surge in sensor networking of oceans created interest in underwater vehicles with both efficient cruising and automated docking capabilities [10]. VRTs may prove to be an ideal solution in such applications. As demonstrated in the following sections, the actuator itself is contained entirely within the vehicle with only a small opening at the surface of the vehicle. Therefore, these control devices would have a minimal impact on the forward drag profile of the vehicle, allowing for long-range travel. Additionally, the placement of these actuators allows for complete thrust vectoring, even when the vehicle has zero forward velocity. This allows for a complete range of motion for docking purposes.

This paper will organize the discussion of these devices in the following manner. Section II will describe the basic concept of the actuator and its inspiration. Section III will discuss the theory behind the thrusters operation. The experimental setup is discussed in Section IV. Section V will present our thrust measurements and describe the thrust characteristics of the thrusters. Concluding remarks will be presented in Section VI.

II. Vortex Ring Thruster

The device examined in this paper was loosely inspired by the natural prolusion schemes of various species of cephalopod and jellyfish. As illustrated in Fig. 1(a), to propel itself through the water, the squid ingests the surrounding fluid into a large mantle cavity. The squid then ejects the fluid with a high momentum through a nozzle near its tentacles called the siphon. The high-energy shear layer rolls into an array of vortex rings, or pulsed jet, and carries the fluid away from the squid. This locomotive technique is the conceptual basis for the thruster studied here, although it should be noted that biological systems operate with pulsation frequencies orders of magnitude lower than our thruster. In addition, squid jet propulsion takes place with a high relative forward velocity, whereas our thrusters operate at low maneuvering speeds much more similar to the locomotion of jellyfish shown in Fig. 1(b).

The VRT can be thought of in similar terms as the squid example. A conceptual diagram of the thruster is shown in Fig. 2(a). The computer-aided design (CAD) model of the actuator and a prototype of our actuator are shown in Fig. 2(b) and (c), respectively. The device consists of a large cavity similar to the mantle with a fluid manipulator inside, which changes the volume of the cavity and forces fluid in and out of an opening at one end. The fluid manipulator used in our thruster is a semiflexible plunger, very similar to an accordion-style bellows. The opening through which the fluid travels is a replaceable part that allows its size to be easily changed. The opening consists of a thin plate with a perfectly circular

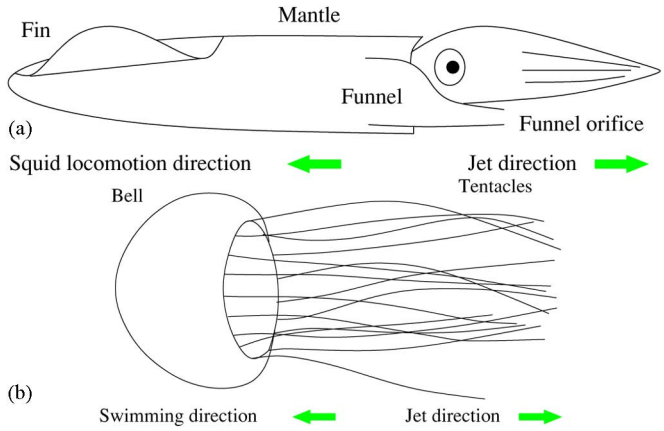

Fig. 1. Conceptual diagram of underwater jet locomotion for both (a) squid and (b) jellyfish.

orifice of minimal surface roughness. The inner edge of the orifice is angled parallel to the flow to avoid nozzle pressure effects. The thruster successively ingests and expels fluid through the same opening. The thruster in this investigation utilizes a mechanical driving mechanism to ensure consistency; however, studies have also been performed using thrusters with solenoid drivers [8] as well as acoustic actuation [11]. The device is very similar to synthetic jet devices used in air for flow control; for more information on synthetic jets see [12]. A unique quality of this type of device is that it has a zero net mass flux over an entire actuation cycle but a positive momentum flux. Much like the squid, the device ingest the low-momentum fluid from its surroundings and ejects it back into the fluid reservoir with a much higher momentum.

III. Theoretical Model

To predict the impulse produced by this type of thruster a modified slug model is derived. Similar to calculations performed by Mohseni and Gharib [13], we assume that the jet comprises a sequence of ejected fluids in a quiescent environment whose impulses are predicted by a slug model. The average jet velocity can be defined in terms of a differential mass transfer across the opening of the cavity as

$$U_j(t) = \frac{\dot{m}}{\rho A} \tag{1}$$

where $\dot{m}$ is the instantaneous mass transfer across the orifice, ρ is the density of the fluid medium, and A is the orifice area. The differential momentum transfer associated with this mass transfer is simply the product of this jet velocity and the differential mass transfer $\dot{m}$. This quantity is also the instantaneous thrust generated by the device

$$T(t) = U_j(t)\dot{m} = \frac{4}{\rho\pi D^2}\dot{m}^2 \tag{2}$$

where T is the instantaneous thrust of the device at any time t. The mass transfer across the opening of the cavity is directly related to the motion of the manipulator within the cavity. As was previously mentioned, the thruster studied here uses an oscillating plunger to actuate the fluid in and out of the cavity. The plunger is mechanically driven, which ensures a constant

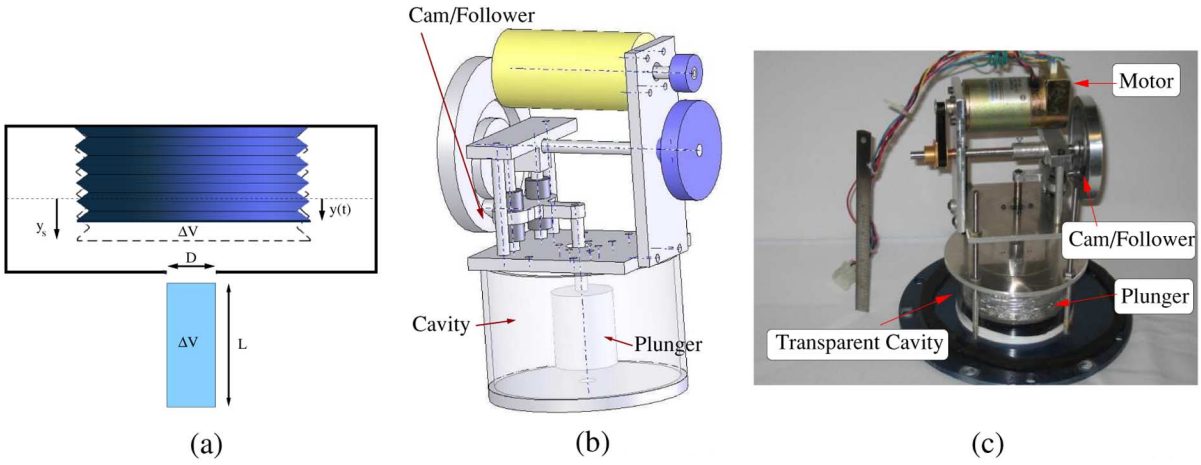

Fig. 2. VRT: theoretical model and actual device. (a) Conceptual model of the actuator. (b) CAD model of the actual device. (c) Actual device.

plunger amplitude y_s and similarly a constant jet volume V. Change in volume is directly related to the plunger deflection; this allows the mass transfer to be easily calculated from the plunger deflection profile $\dot{m} = \rho V(\dot{y}(t)/y_s)$, where $y(t)$ is the plunger deflection as a function of time, and $\dot{y}(t)$ is the rate at which the plunger deflects. The thruster analyzed herein has a sinusoidal plunger deflection profile with frequency f. This means that the thrust achieved with this type of a device is a function of the diameter of the orifice D, the density of the fluid, the volume of the jet, the plunger stroke profile, and the frequency of actuation f. Assuming that the plunger has a constantly controlled stroke profile, the Buckingham Π theorem predicts that the thrust equation should reduce to a function of two nondimensional parameters. The first is a coefficient of thrust defined by

$$C_T = \frac{\bar{T}}{D^4 \rho f^2} \tag{3}$$

where $\bar{T}$ is the average thrust produced over an entire actuation cycle defined as $\bar{T}P = \int_0^{t_e} T(t)dt$. P is the actuation period and t_e is the time required for jet expulsion, which for a plunger stroke profile with a 50% duty cycle is $t_e = (1/2)P = (1/2f)$. The other nondimensional parameter that characterizes the jet pulsation is the ratio of the length to the diameter of the jet (L/D), if the exiting jet were a perfect cylinder. This term is referred to as the "stroke ratio" by Smith and Glezer [14], [15]. The term has also been called the formation time in [16], because it can also be considered as the time that the jet has been ejected nondimensionalized by the jet velocity and jet diameter $(L/D) = \int_0^{t_e} (U_j/D)dt$. This is a useful definition when analyzing the jet pinchoff phenomenon, which will be discussed later in this section.

If the average thrust $\bar{T}$ is calculated assuming the sinusoidal plunger deflection profile used by the thruster, then the average thrust equation is given by

$$\bar{T} = \rho \frac{\pi^3}{16} L^2 D^2 f^2 \tag{4}$$

or in nondimensional terms

$$C_T = \frac{\pi^3}{16} \left(\frac{L}{D}\right)^2. \tag{5}$$

The slug model assumes that all fluids start initially from rest and it ignores the effect that previously formed vortex rings have on the flow field of the jet. This effect should not be ignored given the rapid succession in which jets are expelled. Experiments were performed by Krueger and Gharib [17], which showed that cyclical jet pulsing had the effect of augmenting the jet thrust as much as 1.9 times the thrust produced by a single jet. The thrust augmentation was considered to be caused by overpressure at the nozzle opening and observed to degrade as the stroke ratio and jet expulsion frequency were increased. The device used to generate the jets studied in [17] differs significantly from the thrusters studied in this paper, because the expelled fluid used in [17] was supplied by an external fluid source, whereas the actuator of our investigation ingests its fluid from the surrounding reservoir. The ingestion phase may have the effect of changing the nozzle overpressure. The pulsation dynamics will be accounted for by a correction factor α in the thrust (5), which according to jet pulsation studies should scale as a function of both the formation number and the actuation frequency

$$C_T = \alpha \frac{\pi^3}{16} \left(\frac{L}{D}\right)^2. \tag{6}$$

The slug model is considered here to predict the maximal thrust, which can be generated by the actuator, associated with a maximum momentum transfer. The slug model assumes that all of the fluid being ingested is completely at rest (no momentum), so that the momentum transfer is characterized by the generation of high-momentum fluid during the expulsion phase. The dynamics of the fluid close to the actuator is strongly influenced by a vortex ring phenomenon known as "pinchoff" [16]. It was determined by Gharib *et al.* [16], [18] that there is a characteristic formation time at which the leading vortex ring entrains a maximum amount of circulation and pinches off from the trailing shear flow. This universal time scale was called the "formation

number" and it was reported to lie between 3.6 and 4.5 for various jet velocities (with an impulsive jet ejection profile [16]). These measurements were supported by numerical calculations in [13], which related flow invariants such as nondimensional circulation and energy between vortices in the Norbury family and jets being generated with various exit velocity history. The low circulation trailing vortex ring created by the pinchoff phenomenon lingers very close to the orifice due to its lower induction velocity. Though the trailing jet has a lower momentum than the primary vortex ring, it still has a larger momentum than the surrounding fluid at rest. It is predicted that thrusters operating with stroke ratios larger than the formation number will ingest a portion of the trailing jet instead of the fluid at rest. This will have the effect of reducing the net momentum flux because the ingestion phase has a higher momentum flux, which, in turn, diminishes the thrust production.

A. Vortex Ring Formation and Reynolds Number Dependency

Another crucial nondimensional parameter, which characterizes the jet flow leaving the actuator, is the jet Reynolds number. The Reynolds number of the jet describes the relative significance of viscous damping forces to inertial forces and is closely related to the transition into turbulent flow regimes. The jet Reynolds number can be computed in terms of the initial circulation Γ_0 defined as [19]

$$\Gamma_0 = \int_0^{t_e} \frac{1}{2} U_j^2(t) dt. \tag{7}$$

This quantity is the time integrand of the differential circulation generated at the orifice over the oscillation period of the actuator. In terms of the initial circulation, the Reynolds number becomes

$$\mathrm{Re}_\Gamma = 2\frac{\Gamma_0}{\nu}. \tag{8}$$

A complete derivation of the relation between the initial circulation and the characteristic velocity/length of the hypothetical cylindrical slug of fluid is given in [19]. It was determined that jets created from fluid at rest will roll into laminar vortex rings if the Reynolds number is less than a critical Reynolds number, which is dependent on the stroke ratio of the jet. For a jet with a stroke ratio of 2.3, the critical Reynolds number at which the vortex ring becomes turbulent is 25 000 [19].

To analyze the nature of the jet a cross section of the flow extruding from the thruster was photographed using a laser-induced fluorescein (LIF) technique. A laser sheet was used to illuminate the vortex ring cross section shown in Fig. 3. According to the formulation of the Reynolds number in terms of the initial circulation, every pulse of the thruster at the operational parameters used in capturing the images in Fig. 3 produces a ring with an identical Reynolds number of 9408. The first ejected vortex ring is clearly seen to be a laminar one. This ring is created from a laminar jet extruding from the orifice [Fig. 3(a)]. For this ring, the Glezer criteria for the laminarity of the vortex ring is clearly satisfied. It should be noted that all of the vortex rings studied in [19] were started from laminar jets, whereby fluid at rest in a cylinder was ejected by a sliding piston, which was reset and brought to rest before subsequent testing. The jet only evolved into a turbulent ring if a critical Reynolds number criterion was met. The second ring ejected from our thruster, by contrast, started from a turbulent jet and evolved into a turbulent ring. Even though the Re_Γ for both rings is identical for both cases, $\mathrm{Re}_\Gamma = 9408$, the second ring is clearly turbulent because it is generated from a turbulent jet (the jet is initially turbulent because it comprises fluid, which was recently ingested into the cavity). The inherent disturbances in the cycling fluid motion into the cavity causes pulsatile jets to be much more prone to turbulence than starting jets, an idea reflected in the higher spreading rate of a pulsatile jet as compared with a steady jet.[1] Therefore, in all of the experiments conducted in this investigation, the emanating jet from the orifice is primarily turbulent.

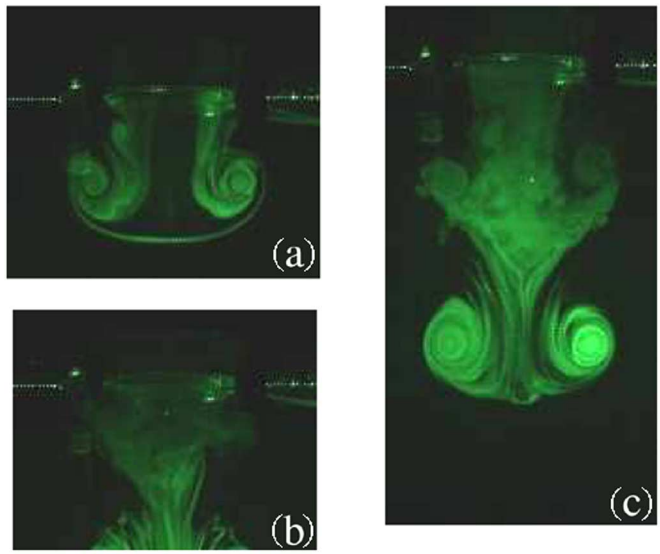

Fig. 3. Cross section of the flow emanating from thruster operating with stroke ratio of 2.3 and $f = 7$ Hz. A reflective dye is illuminated with a laser sheet through the center of the vortex ring. (a) Initial ring with a laminar starting jet. (b) Secondary turbulent pulsatile jet . (c) Both fully evolved vortex rings.

IV. Experimental Setup

The experimental setup for this research comprises three primary components, whose operational relationship is shown in Fig. 4. The first is the thrust actuator itself, the second is the tank that houses a fluid reservoir and provides the necessary reaction forces for our load cell, and the third is a data acquisition assembly. To measure the thrust, the test actuator is sealed within a transparent canister, which is submerged fully within the fluid reservoir in the testing tank. A vertical rod runs from the canister to a frame mounting structure keeping the thruster stationary and translating the forces to the force sensor, where the thrust signal is recovered.

A. Thrust Actuator

The actuator used in our tests for thrust characterization is much larger and more versatile than an actuator which would be installed in a vehicle. The actuator can be considered analogous

[1]For experimental measurement and analytical modeling of microsynthetic jets in air, see [20]

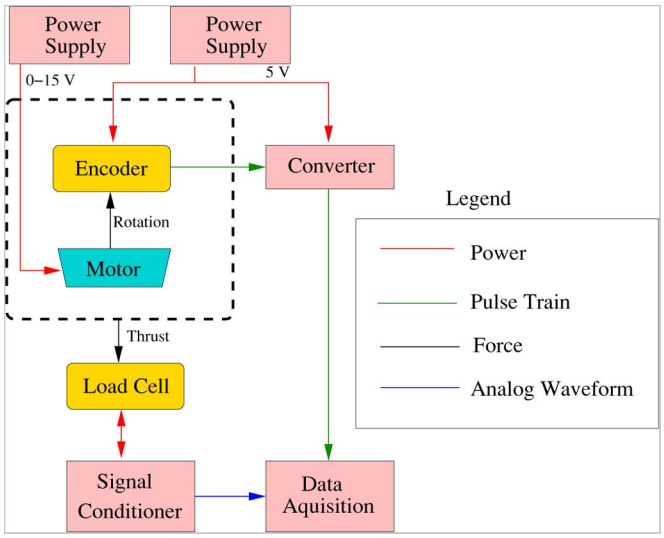

Fig. 4. Testing setup functional block diagram.

Fig. 5. Actuator testing tank.

to the theoretical actuator model depicted in Fig. 2. An oscillating plunger is suspended in a wide fluid cavity. The plunger is driven by the following mechanical system. A high torque motor is used to drive the rotation of a cam, whose track forces a follower up and down periodically. The follower rides on a set of linear bearings, which restrict its motion to a linear path. The plunger is connected directly to this follower. As the plunger pulses up and down, it forces fluid in and out of the cavity through a small opening at the bottom. The shape of the cam track controls the fluid slug volume and mass flux profile. The cam used to generate data for this paper utilizes a basic sinusoidal stroke profile, with a magnitude of 6.35 mm, in which 41.5 mL of water is expelled every pulse. The plunger itself is made of a sealed length of flexible ducting. The entire assembly is encased in a sealed canister and then submerged in the fluid reservoir.

B. Testing Environment

The water tank, which houses the fluid reservoir, was designed and fabricated by our group specifically for this investigation, and is depicted in Fig. 5. It is 2.13 m tall, and 0.91 m $\times$ 1.22 m in cross section and houses 2.38 kL of water. The tank is made out of acrylic to allow for visual access from all angles (including the bottom of the tank), and it is supported by an outer steel skeleton. At the top of the tank is a mounting structure, which is securely attached to the outer frame. This mounting structure contains a set of linear bearings, which restrict the actuator's lateral motion, while allowing the axial thrust to be translated through the connecting rod to the force sensor. Also contained on the mounting structure is a mounting bracket, which holds our force sensor and provides a rigid constraint for proper sensor measurement.

C. Data Acquisition

The load sensor used intrinsically is a PCB 1102 load cell canister. The load cell is actually an optimized arrangement of several strain gauges, making it a static sensor with a 445-N load limit with 2.5% sensitivity. When running our tests, the data acquisition assembly records motor encoder data as well as a thrust waveform from the load cell. The motor encoder outputs a quadrature clock signal, which is filtered and converted to a single pulse train to simplify the recording process. The load cell canister is powered, filtered, and interpreted by a signal conditioning box. The signal conditioner outputs a direct current (dc) voltage waveform, which corresponds to the actuator thrust. Both signals are recovered via a National Instruments (Austin, TX) data acquisition card. The system is programmed to successively count the pulse train to give a motor frequency reading at 1 Hz and sample the analog waveform at 10 kHz.

V. Results

A. Actuator Thrust Characteristics

The model developed in Section III predicts that the thrust generated by the thruster is dependent on the frequency of the jet and the size and pulsation time of the jet (described by jet diameter and stroke ratio). The first actuation parameter tested was the jet expulsion frequency. The test actuator was mechanically driven to ensure that the plunger deflected to a constant distance independently of any other constraints. Additionally, the plunger was rigorously designed to ensure consistent volume deflection (jet volume), for a given plunger deflection. The replaceable orifice through which the jets are ejected was kept constant to allow the frequency to be independently tested for a constant stroke ratio. The dependence of the actuator thrust to actuation frequency f is depicted in Fig. 6. This graph depicts the thrust generated by the actuator at various actuation frequency with a nozzle diameter corresponding to a stroke ratio of 3.0. It should be noted that the pulsatile nature of the device causes the thrust to be very dynamic over the entire actuation cycle. All of the thrust results presented in this section are taken

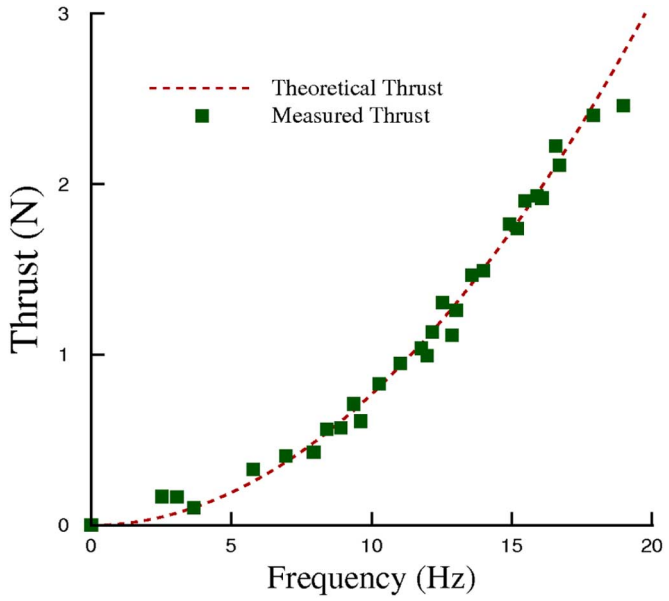

Fig. 6. Average actuator thrust versus frequency at $L/D = 3.0$. Theoretical curve derived in (4).

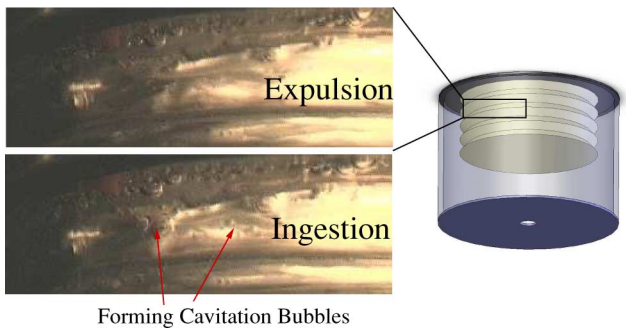

Fig. 7. Cavitation bubbles within cavity of thruster operating with $f = 17$ Hz and $L/D = 4.3$.

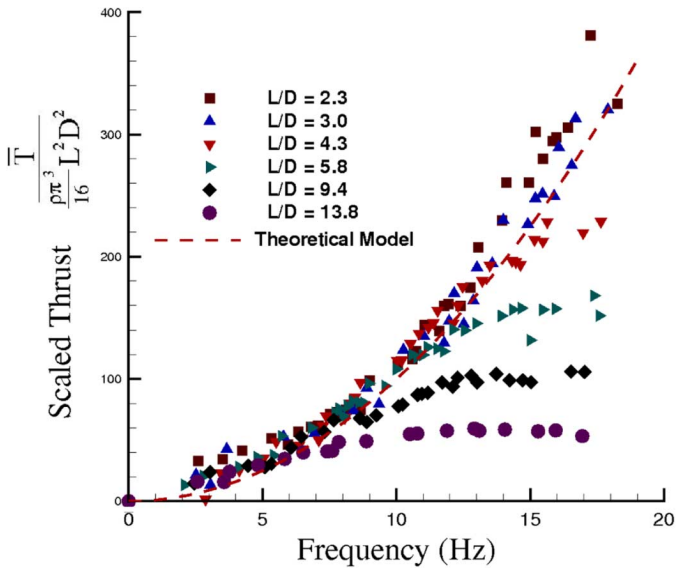

Fig. 8. Thrust is plotted on the frequency domain for the entire range of stroke ratios tested.

by averaging this thrust over a sufficiently long period of time to give a single thrust value.

In addition to the empirical thrust response curve, Fig. 6 depicts the theoretical thrust response, which was predicted by the slug momentum model described in (4). It can be seen that the actual frequency response of the actuator is proportional to the square of the frequency, which is in excellent agreement with the slug model.

It should be noted that the testing was only conducted up to a frequency of ≈ 20 Hz. At higher frequencies, we observed evidence of cavitation inside the actuator cavity. Cavitation is an effect not predicted by our simplistic slug model. When the actuator frequency becomes critically high, the pressure drop taking place during the fluid ingestion phase causes the water close to the piston to expand into small cavitation bubbles. Through the use of a high-speed camera (Phantom v4.3 with a wide angle lens), this phenomenon was captured visually. Fig. 7 shows a closeup image of the piston within the thruster cavity during both phases of actuation (ingestion and expulsion). The actuator is operating with a stroke ratio of 4.3 and a frequency of 17 Hz. The lower part of the image shows the piston just after the ingestion stroke causes a pressure drop resulting in the formation of cavitation bubbles. The upper part of the image shows the piston just after the ejection stroke. Some of the bubbles remain at the top of the piston, but many of them have imploded due to the sudden increase in pressure. This cycle has the effect of reducing the size of the ejecting jet since part of the volume change induced by the plunger deflection goes into collapsing the cavitation bubbles instead of ejecting fluids from the orifice. Additionally, implosion of the cavitation bubbles results in unpredictable forces acting on the piston. Therefore, testing was terminated when the increasing frequency resulted in cavitation.

The thrust response with respect to frequency was tested for a range of stroke ratios up to 14. In Fig. 8, the thrust measured for each stroke length has been plotted versus the actuation frequency. It is observed that for higher stroke ratio the thrust saturates after a critical frequency is reached. This critical frequency decreases as the stroke ratio is increased. This phenomenon is attributed to the cavitation formation inside the cavity. For a constant stroke ratio, as the actuation frequency increases, a higher pressure drop inside the cavity is expected in order to deliver higher jet flow rates. As a result, the flow inside the cavity is more prone to cavitation at higher frequencies. It should be noted that before cavitation the thrust response curves maintain a strong dependency on the square of the frequency, as predicted by (4).

The nondimensionalization theory described in Section III predicts that the values of the thrust produced at any actuation frequency should converge upon a single coefficient of thrust as long as the stroke ratio is held constant. For each stroke ratio tested, the entire range of thrust measurements at various frequencies was scaled by the actuation frequency and orifice diameter to give the coefficient of thrust described in (3). The average coefficient of thrust measured for several stroke ratios has

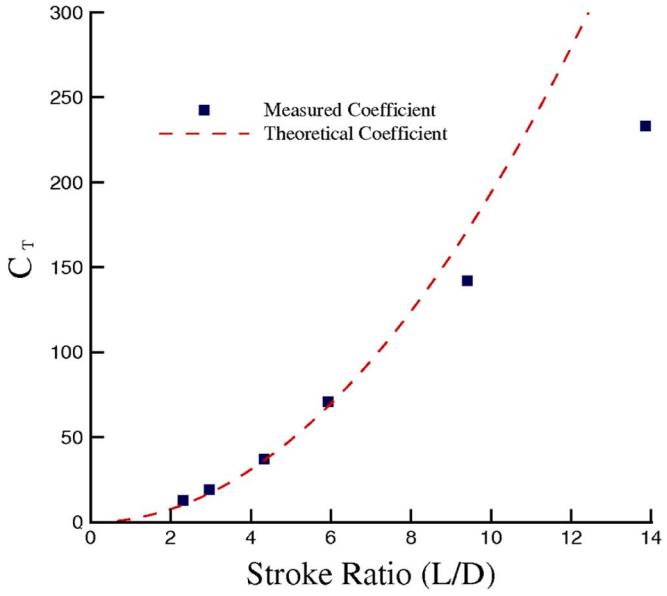

Fig. 9. Theoretical and measured thrust coefficient as a function of the stroke ratio.

been plotted in Fig. 9. In addition, the graph contains the theoretical thrust coefficient as a function of the stroke ratio, as predicted by (5).

The coefficient of thrust described in (5) is in good agreement with the measured coefficients for stroke ratios up to ≈ 7 at which point the accuracy of the model degrades with the increasing stroke ratio. This loss of thrust accuracy could be attributed to the pinchoff effect. As the stroke ratio increases beyond the formation number, the shear flow that pinches off from the primary vortex ring forms a trailing ring with a much lower induction velocity. This causes the ring to linger close enough to the actuator that some of the jet is ingested back into the cavity, degrading the momentum transfer of the device. As the stroke ratio increases, the amount of the jet left in the trailing ring also increases resulting in a greater loss in momentum transfer.

The fact that each stroke ratio is represented by a single point in Fig. 9 is misleading. This would suggest that all the thrust data for every formation number converges to a single coefficient of thrust. This is generally true for the thrust measured with stroke ratios below the formation number; however, the thrust coefficient measured for stroke ratios greater than the formation number showed a strong dependency on frequency, and the average was reported. The scale factor α, which was defined as a correction factor to the slug model as shown in (6), shows the accuracy of the slug model for various actuation parameters. Fig. 10 shows the scale factor for the actuator thrust coefficient for every stroke ratio over the entire frequency range. The graph is separated into two parts. Fig. 10(a) shows the scale factor for stroke ratios below the formation number, whereas Fig. 10(b) shows the scale factor for stroke ratios above the formation number. For stroke ratios below the formation number, the scaling factor α is almost unity over the range of frequencies investigated in this study [see Fig. 10(a)]. However, the thrust coefficient dependency on frequency is shown to become a monotonically decreasing function of frequency as the stroke ratio increased above the formation number [see Fig. 10(b)]. Furthermore, for the stroke ratio cases where this dependency is observed (those above the formation number), the thrust coefficient decreases proportional to the frequency. This is attributed to the fact that at stroke ratios above the formation number the leading vortex ring does not ingest any more of the emanating jet; consequently, the resulting trailing jet is more prone to be redrawn into the cavity during the ingestion cycle. As a result, the averaged thrust over a full pulsation cycle is seen to be reducing. This clearly shows that from a thrust generation view point, it is beneficial to operate a VRT around its formation number.

When considering the thruster parameter selection in vehicle design, the loss in momentum flux should be avoided by selecting a stroke ratio equal to the formation number. This will give a thrust coefficient that is accurate to an upper bound frequency defined by the cavitation frequency. Another design consideration that must be taken into account is the fact that the thrusters will be operating in environments which are not at rest. As the actuator delivers a thrust to the vehicle, the vehicle will move forward through the surrounding fluid. As a result, a background velocity in the direction of the jet could be observed. The effects of this coflow on vortex ring formation were studied by Krueger in [21]. He reports that vortex rings being generated with a uniform background coflow will experience pinchoff at a much lower formation time (stroke ratio) as the coflow velocity approaches the jet velocity. Because the thrust coefficient was shown to degrade as the stroke ratio surpassed the formation number for the jet, thrusters to be used in vehicles should be designed with a stroke ratio below the static formation number to avoid loss in thrust coefficient from coflow effects while in motion.

B. Thrust Tracking Response

Typical propellor thrusters have an accurate thrust output for a given rotational velocity under steady-state conditions. However, the thruster has a time delay associated with reaching a given control force. This time delay grows inversely with the magnitude of the desired force [2]. Typical forces were reported in [2] to require between 2 and 5 s to settle on the steady thrust value. This causes thruster forces to be very unpredictable when creating short impulsive forces, which are required for station keeping. For a thruster to be effective at keeping a vehicle in a loiter position, it must have a settling time that is much smaller than the time associated with the oscillating flow of dynamic environments. It was presented in [22] that propellor thrusters, which were operated at low rotational frequencies and which changed direction rapidly, produced a range of forces that even included forces in the opposite direction of the desired force. This is because propellor response is highly dependent on the velocity of the fluid it is interacting with. In addition to the delay associated with reaching the given force, typical devices have a delay associated with terminating the thrust [7]. This is because propellor-type thrusters generate thrust from inducing a steady flow in a given direction; therefore, the thrust will deviate from the desired/modeled level whenever the flow is in a transient state. The time delays associated with propellor thrust induce a limit cycle in the vehicle control scheme, which is often larger than the required positioning accuracy for ocean

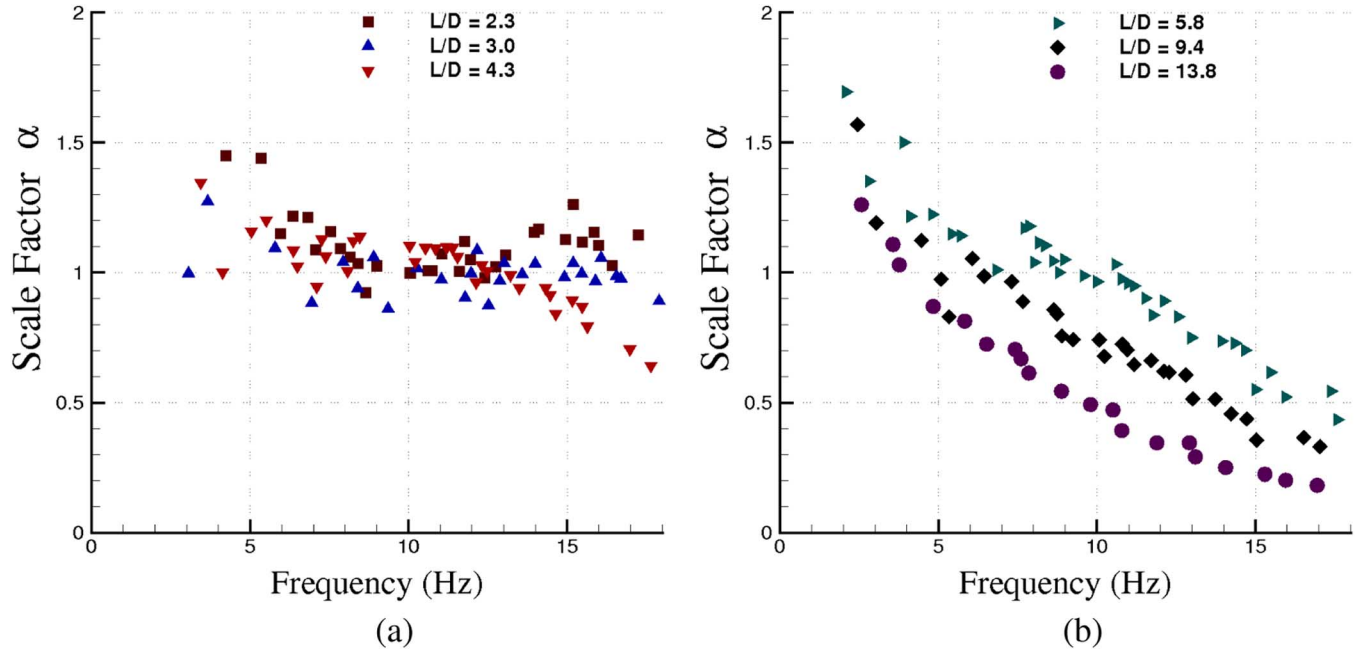

Fig. 10. Scale factor α defined on the actuator frequency domain for (a) stroke ratios below the formation number and (b) stroke ratios above the formation number.

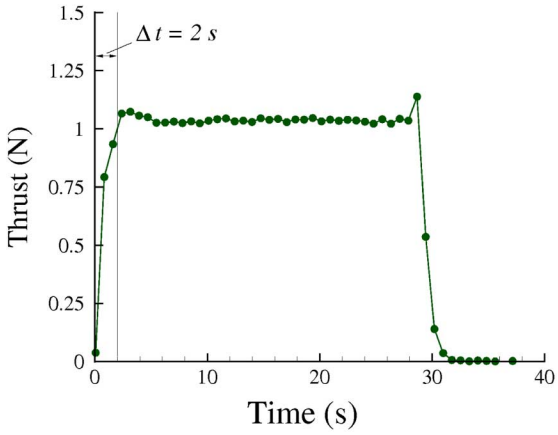

Fig. 11. Thrust response of VRT with respect to time.

mapping or docking vehicles. This limit cycle can be reduced with higher order sliding controllers [2], but these methods require extremely accurate state determination, which may not be practical for typical applications. Therefore, systems requiring high positioning accuracy will require a thruster with more predictable force outputs for impulsive-type actuation.

One significant benefit of the VRT in this investigation is that it reaches steady-state thrust values quickly. Fig. 11 shows the average thrust generated by a vortex-generating thruster from ignition through several actuation cycles. It can be seen that the thruster reaches static values in the order of 2 s, and reached 80% of the static value within 0.5 s. This particular case was recorded with a stroke ratio of 5.9 and an actuation frequency of 8.75 Hz; however, this thrust settling time was seen to be typical for the entire range of tested driving parameters, unlike the nonlinear settling response time of propellor thrusters. This indicates that the observed settling time is caused by a mechanical delay and not by propulsion dynamics. The time delay associated with thrust termination is similarly small so that the vehicle receives the exact amount of controlling force prescribed by the control architecture. Furthermore, because the thrust is delivered in independent pulses, the prescribed thrust can be quantized to any level without inducing additional dynamics, which simplifies the complexities associated with using layered controls due to thruster nonlinear dynamics [23] (the lower limit of this quantizable thrust being defined by the impulse of a single jet). The immediate desired thrust tracking of these devices can significantly reduce the loitering limit cycles of aquatic robots during station keeping missions in dynamic environments. Furthermore, the ejecting jet for the range of parameters studied here is always turbulent. As a result, the jet characteristics observed in this paper are predicted to hold true irrespective of the laminar/turbulent nature of the surrounding fluid.

C. Colorado Underwater Robotic Testbeds

The University of Colorado, Boulder, has developed several generations of vehicles to test the feasibility of this type of thruster technology within a vehicle system architecture.

The most recent vehicle, named Cavity Actuated Low-Speed Actively Maneuvering Aquatic Rover Experiment (CALAMAR-E), shown in Fig. 12, utilized vortex-generating thrusters without any control surfaces whatsoever. The vehicle was 1.45 m long, 21.1 cm in diameter, and had a total mass of 49.9 kg. The optimal stroke ratio reported in Section V-A was incorporated as design parameters for the thrusters built for the vehicle. These actuators were tested independently in the testing tank of Fig. 5, as well as in the vehicle architecture. Within the stationary testing tank environment, the compact thrusters were measured to attain a maximum thrust of 0.85 N at the optimal operating conditions, and took up approximately 983 cm^3. When two of these actuators were fired at diagonal

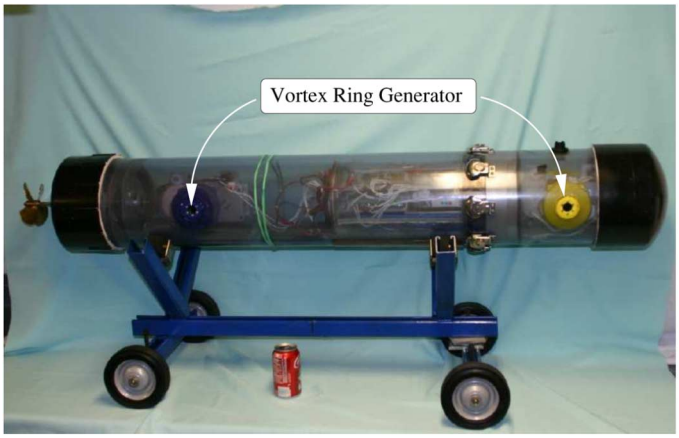

Fig. 12. CALAMAR-E vortex-generating thruster technology demonstrator.

positions, the thrusters induced a vehicle rotation of 2.23 r/min. It should be noted that the vehicle can induce sideways translational motion and rotation completely independent of any other type of motion, which allowed the vehicle to perform a high-accuracy parallel parking maneuver, qualitatively enforcing the maneuvering capability of these thrusters. This maneuver was captured on video, and three successive snapshots were extracted to illustrate the procedure. These snapshots are depicted in Fig. 13. In Fig. 13(a), the vehicle brings itself within proximity of a mock parking structure. In Fig. 13(b), the actuators induce a zero turning radius rotation to bring the vehicle into parallel alignment with the parking structure. In Fig. 13(c), the actuators cease rotation and induce a pure sideways translation to bring the vehicle into its proper docking position.

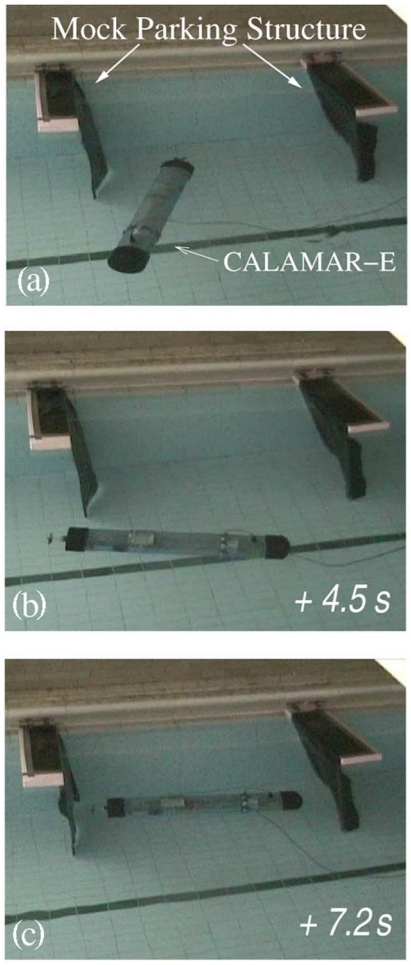

Fig. 13. Successive snapshots of CALAMAR-E performing a parallel park. (a) Alignment with parking structure. (b) Rotation into parallel alignment. (c) Translation into docking position.

VI. Conclusion

Unmanned vehicle networks are becoming an irreplaceable resource for in depth scientific testing in oceanic environments. Current vehicles are limited by an inability to provide simultaneous docking and transit capabilities. A new type of underwater jet thruster called a VRT offers a possible solution to this problem because it offers faster tracking and lower drag than typical propellor thrusters, while maintaining the thrust capabilities at zero forward velocity.

The parameters controlling the operation of this type of thruster are identified. From these parameters, a fluid slug model was developed to predict the thrust. It was observed that the model predicts the thrust accurately for devices operating at frequencies below the cavitation frequency and stroke ratios below the formation number. To verify the accuracy of this model, a versatile actuator was designed and built, which had the capability to adjust all of the parameters independently. It was empirically determined that these devices have optimal thrust characteristics when pulsing jets with a stroke ratio equal to the formation number when the actuation frequency approaches the critical value associated with fluid cavitation.

Flow visualization and thrust characterization experiments were conducted for the VRT actuators. These visual experiments demonstrated pulsating jets susceptibility to turbulence, and also verified the existence of fluid cavitation at higher frequencies.

Actuator time response was investigated and it is argued that VRTs provide a controlled quantized thrust value with a constant response time faster than the settling time associated with most propellor-style thrusters. A testbed was designed in order to test the thrusters performance in a dynamic vehicle environment. The thrusters were determined to successfully induce rotation and sideways translation in this testbed by performing a parallel park maneuver.

Acknowledgment

The authors would like to thank all the members of the CALAMAR-E 2005/2006 senior project team: C. Turansky, T. Schultz, T. Curtis, S. Delanda, B. McArdle, S. Reed, D. Koblick, and J. Denard. They would also like to thank C. Turansky and T. Clark for contributions to the experimental setup and testing.

References

[1] L. L. Whitcomb, D. R. Yoerger, H. Singh, and D. A. Mindell, "Towards precision robotic maneuvering, survey, and manipulation in unstructured undersea environments," in *Proc. 8th Int. Symp. Robot. Res.*, London, U.K., 1998, pp. 1–11.

[2] D. Yoerger, J. Cooke, and J.-J. Slotine, "The influence of thruster dynamics on underwater vehicle behavior and their incorporation into control system design," *IEEE J. Ocean. Eng.*, vol. 15, no. 3, pp. 167–178, Jul. 1990.
[3] J. Bellingham and J. Wilcox, "Optimizing AUV oceanographic surveys," in *Proc. Autonom. Underwater Veh. Technol.*, Monterey, CA, 1996, pp. 391–398.
[4] H. Singh, J. Bellingham, F. Hover, S. Lemer, B. A. Moran, K. von der Heydt, and D. Yoerger, "Docking for an autonomous ocean sampling network," *IEEE J. Ocean. Eng.*, vol. 26, no. 4, pp. 498–514, Oct. 2001.
[5] N. E. Leonard, D. A. Paley, F. Lekien, R. Sepulchre, D. M. Fratantoni, and R. E. Davis, "Collective motion, sensor networks, and ocean sampling," *Proc. IEEE*, vol. 95, no. 1, pp. 48–74, Jan. 2007.
[6] J. Bellingham, C. Goudey, T. Consi, J. Bales, D. Atwood, J. Leonard, and C. Chryssostomidis, "A second generation AUV," in *Proc. Autonom. Underwater Veh. Technol.*, Cambridge, MA, 1994, pp. 148–155.
[7] M. B. Mclean, "Dynamic performance of small diameter tunnel thrusters," Ph.D. dissertation, Dept. Mech. Eng., Naval Postgrad. Schl., Monterey, CA, 1991.
[8] K. Mohseni, "Pulsatile jets for unmanned underwater maneuvering," in *Proc. 3rd AIAA Unmanned Unlimited Tech. Conf. Workshop Exhibit*, Chicago, IL, Sep. 2004, vol. 20–23, paper 2004-6386.
[9] K. Mohseni, "Pulsatile vortex generators for low-speed maneuvering of small underwater vehicles," *Ocean Eng.*, vol. 33, no. 16, pp. 2209–2223, 2006.
[10] H. Singh, M. Bowen, F. Hover, P. LeBas, and D. Yoerger, "Intelligent docking for and autonomous ocean sampling network," in *Proc. MTS/IEEE OCEANS Conf.*, Halifax, NS, Canada, 1997, pp. 1126–1131.
[11] A. Polsenberg-Thomas, J. Burdick, and K. Mohseni, "An experimental study of voice-coil driven synthetic jet propulsion for underwater vehicles," in *Proc. MTS/IEEE OCEANS Conf.*, Washington, DC, Sep. 19–23, 2005, pp. 923–927.
[12] A. Glezer and M. Amitay, "Synthetic jets," *Ann. Rev. Fluid Mech.*, vol. 34, pp. 503–529, 2002.
[13] K. Mohseni, H. Ran, and T. Colonius, "Numerical experiments on vortex ring formation," *J. Fluid Mech.*, vol. 430, pp. 267–282, 2001.
[14] B. Smith and A. Glezer, "The formation and evolution of synthetic jets," *Phys. Fluids*, vol. 10, no. 9, pp. 2281–2297, 1998.
[15] B. Smith and A. Glezer, "Jet vectoring using synthetic jets," *J. Fluid Mech.*, vol. 458, pp. 1–34, 2002.
[16] M. Gharib, E. Rambod, and K. Shariff, "A universal time scale for vortex ring formation," *J. Fluid Mech.*, vol. 360, pp. 121–140, 1998.
[17] P. Krueger and M. Gharib, "Thrust augmentation and vortex ring evolution in a fully pulsed jet," *AIAA J.*, vol. 43, no. 4, pp. 792–801, 2005.
[18] K. Mohseni and M. Gharib, "A model for universal time scale of vortex ring formation," *Phys. Fluids*, vol. 10, no. 10, pp. 2436–2438, 1998.
[19] A. Glezer, "The formation of vortex rings," *Phys. Fluids*, vol. 31, no. 12, pp. 3532–3542, 1988.
[20] Y. Vargas, T. Finley, K. Mohseni, and J. Hertzberg, "Flow characterization of a synthetic jet," in *Proc. 44th AIAA Aerosp. Sci. Meeting Exhibit*, Reno, NV, Jan. 9–12, 2006, paper 2006-1422.
[21] P. Krueger, J. Dabiri, and M. Gharib, "The formation number of vortex rings formed in a uniform background co-flow," *J. Fluid Mech.*, vol. 556, no. 1, pp. 147–166, 2006.
[22] A. Healey, S. Rock, S. Cody, D. Miles, and J. Brown, "Toward an improved understanding of thruster dynamics for underwater vehicles," *IEEE J. Ocean. Eng.*, vol. 20, no. 4, pp. 354–361, Oct. 1995.
[23] J. Bellingham, T. Consi, R. Beaton, and W. Hall, "Keeping layered control simple," in *Proc. Autonom. Underwater Veh. Technol.*, Washington, DC, 1990, pp. 3–8.

Michael Krieg (S'08) received the B.S. degree in aerospace engineering sciences from the University of Colorado at Boulder, where he is currently working towards the Ph.D. degree.

His areas of interest include hydrodynamic design, multiple vehicle cooperative control, and novel propulsive schemes.

Kamran Mohseni (M'06) received the B.S. degree in mechanical engineering from the University of Science and Technology, Tehran, Iran, in 1990, the M.S. degree in aeronautics from the Imperial College of Science, Technology, and Medicine London, U.K., in 1993, and the Ph.D. degree in mechanical engineering from the California Institute of Technology (Caltech), Pasadena, in 2000.

Currently, he is an Associate Professor in Aerospace Engineering Sciences at the University of Colorado at Boulder, which he joined in 2001 after a year as a Postdoctoral Fellow in Control and Dynamical Systems at Caltech. His research interests are in microscale transport, vortex dynamics and biomimetic, and fluidic locomotion.

Dr. Mohseni is a member of the American Society of Mechanical Engineers (ASME), the American Physical Society (APS), the Society for Industrial and Applied Mathematics (SIAM), and the American Institute of Aeronautics and Astronautics (AIAA).